RL-TR-91-270
In-House Report
August 1991

ADAPTIVE OPTICAL PROCESSOR

Michael J. Ward, Capt, USAF; Christopher W. Keefer, Capt, USAF;
Dr. Stephen T. Welstead

APPROVED FOR PUBLIC RELEASE; DISTRIBUTION UNLIMITED.

Rome Laboratory
Air Force Systems Command
Griffiss Air Force Base, NY 13441-5700

This report has been reviewed by the Rome Laboratory Public Affairs Office (PA) and is releasable to the National Technical Information Service (NTIS). At NTIS it will be releasable to the general public, including foreign nations.

RL-TR-91-270 has been reviewed and is approved for publication.

APPROVED:

ANDREW R. PIRICH, Acting Chief
Photonics & Optics Division

FOR THE COMMANDER:

DONALD W. HANSON, Director
Surveillance & Photonics Directorate

If your address has changed or if you wish to be removed from the Rome Laboratory mailing list, or if the addressee is no longer employed by your organization, please notify RL(OCPA) Griffiss AFB NY 13441-5700. This will assist us in maintaining a current mailing list.

Do not return copies of this report unless contractual obligations or notices on a specific document require that it be returned.

REPORT DOCUMENTATION PAGE

Form Approved
OMB No. 0704-0188

1. AGENCY USE ONLY (Leave Blank)	2. REPORT DATE	3. REPORT TYPE AND DATES COVERED
	August 1991	In-House Feb 89 - Jan 91

4. TITLE AND SUBTITLE
ADAPTIVE OPTICAL PROCESSOR

5. FUNDING NUMBERS
PE - 62702F
PR - 4600
TA - P1
WU - 03

6. AUTHOR(S)
Michael J. Ward, Capt, USAF; Christopher W. Keefer, Capt, USAF; Dr. Stephen T. Welstead

7. PERFORMING ORGANIZATION NAME(S) AND ADDRESS(ES)
Rome Laboratory (OCPA)
Griffiss AFB NY 13441-5700

COLSA, Inc.
6726 Odyssey Drive
Huntsville AL 35806

8. PERFORMING ORGANIZATION REPORT NUMBER
P9-H010

9. SPONSORING/MONITORING AGENCY NAME(S) AND ADDRESS(ES)
Rome Laboratory (OCPA)
Griffiss AFB NY 13441-5700

10. SPONSORING/MONITORING AGENCY REPORT NUMBER
RL-TR-91-270

11. SUPPLEMENTARY NOTES
Rome Laboratory Project Engineer: Michael J. Ward, Capt, USAF/OCPA/(315) 330-2944

12a. DISTRIBUTION/AVAILABILITY STATEMENT
Approved for public release; distribution unlimited.

12b. DISTRIBUTION CODE

13. ABSTRACT (Maximum 200 words)

The Phase I in-house effort to develop an optical processor as an electronic counter-counter-measure for radar multipath is discussed. The closed loop system demonstrates the ability to achieve a 15.2+/-2.4 dB adaptive cancellation of a single tone, single delay jamming signal over a 1-5 MHz bandwidth. The open loop optical system proves capable of providing a 30.2+/-3.9 dB cancellation of the same signal when using operator provided information. Key elements of this project include the characterization and selection of a spatial light modulator (SLM) system and the development of a software package which assists the minimization process. This has resulted in the novel use of a two dimensional binary SLM to perform as an enhanced grey scale one dimensional SLM. Additionally, an acousto-optic (AO) deflector has been demonstrated to provide the grey level dynamic range and spatial resolution required by the system. The results of this single channel testbed will be used in the future development of a multichannel optical processor.

14. SUBJECT TERMS
Optical processing, Adaptive algorithms, Adaptive nulling, Acousto-optics

15. NUMBER OF PAGES
48

16. PRICE CODE

17. SECURITY CLASSIFICATION OF REPORT	18. SECURITY CLASSIFICATION OF THIS PAGE	19. SECURITY CLASSIFICATION OF ABSTRACT	20. LIMITATION OF ABSTRACT
UNCLASSIFIED	UNCLASSIFIED	UNCLASSIFIED	U/L

NSN 7540-01-280-5500

Standard Form 298 (Rev. 2-89)
Prescribed by ANSI Std. Z39-18
298-102

Table of Contents

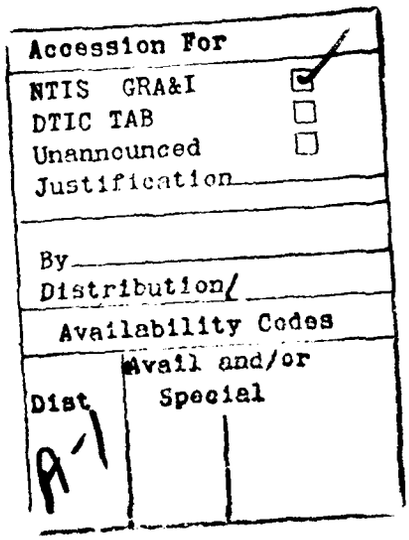

List of Figures

List of Tables

1. Introduction

1.1 Requirements. Multipath sidelobe jamming is a problem faced by Air Force radar systems on the electronic battlefield. Electronic sidelobe cancelers have been developed as a countermeasure to sidelobe jamming. However, these cancelers are limited in their ability to adapt to changes in the jamming signal, in their ability to successfully defeat multipath jamming signals with discrete tapped time delay lines, and in their ability to handle bandwidths greater than 1 MHz. Hence the need exists for a signal processor which can adapt to the rapidly changing delays of wideband multipath sidelobe jamming. We believe this need can be satisfied with an optically based signal processing system by exploiting the ability of optical systems to perform high speed parallel computations and the advantage of using acousto-optical devices to serve as continuously variable tapped time delay lines.

1.2 Overview of Five Year In-House Plan. The five year plan to develop a functional electro-optic testbed to meet operational requirements is composed of three project phases, as diagrammed in Figure 1. The goal of Phase I is to demonstrate the concept of using an electro-optic architecture to adaptively process a single delay from a monotone signal source. The design, fabrication, and testing results of a single channel (ie., single jamming source) optical processing system are documented in this Phase I final report.

Phase II consists of the design and fabrication of a multi-channel adaptive optical processor (MADOP), which will be designed to meet operational specifications. Initial plans call for a dual channel system which will later be upgraded to a four channel system. The MADOP will be designed to be portable and rugged enough for transportation to a test location.

During Phase III, we plan to test and evaluate the completed MADOP both in the lab and in the field. These tests will be designed to measure the ability of this optical processing architecture to satisfy operational requirements for adaptive signal processing.

1.3 Background. This report documents the Phase I in-house research effort to design, build, and test a single channel optical signal processor. The effort, JON 4600-P103, entitled "Adaptive Optical Processor", began OCT 1988 in the Analog and Lightwave Optical Signal Processing Division of the Photonics Center at the Rome Laboratory, Griffiss AFB, NY. It has been supported by two Expert in Science and Engineering (ESE) contracts, "Hybrid Electro-Optical Processor" (contract #F30602-88-D-0027) and "Test and Evaluation of Optical Signal Processor" (contract #F30602-88-D-0028), both performed by Dr. Stephen Welstead, an applied mathematician, of COLSA, Inc. during FY89 and FY90. The ESE support has been directed towards modeling the proposed optical implementation performance and developing computer algorithms to improve the system's adapting capability. The design, fabrication, and testing of the

optical system has been performed by in-house personnel.

The authors wish to acknowledge the help of several scientists and engineers within the Rome Laboratory who provided assistance at critical points throughout this project: Mr. David Grucza who provided the idea and the initial optical layout of the acousto-optic deflector device used as a spatial light modulator, Dr. George Brost and 1LT Edward Toughlian who helped "trouble-shoot" many of the problems that came up, Mr. Paul Repak and Mr. Wesley Foor who provided programming expertise, and to Mr. Andrew Pirich, Chief of the Analog and Lightwave Optical Signal Processing Division, who provided guidance throughout the project.

1.4 Organization of Paper. The paper first overviews the concept of performing this processing task with an optical system in Section 2. Next, the various algorithm approaches that have been considered are summarized in Section 3, the details are contained in Welstead's ESE final reports[1,2]. The system architecture is described in Section 4. Section 5 describes the various spatial light modulators that were compared for their performance within the system. Test results performed on the optical processor are presented in Section 6. These results are analyzed and conclusions are drawn in Section 7.

2. Optical Processor Concept

2.1 The Scenario. Consider the scenario of elementary *multipath sidelobe jamming* depicted in Figure 2. A main antenna receives the target signal, s(t), into the main lobe with gain G_A, and the multipath jamming signal, $n_1(t)$, into a sidelobe with gain G_B, where $G_A >> G_B$. $n_1(t)$ is a unique compilation of multipath versions of the jamming source j(t). The smaller sidelobe gain offsets the larger magnitude of the jamming source, such that the products $G_A * s(t)$ and $G_B * n_1(t)$ are of similar magnitude. Hence, we define the total signal from the main antenna as d(t), where

$$d(t) = (G_A * s(t)) + (G_B * n_1(t)) \qquad (1)$$

The auxiliary antenna is omnidirectional and thus receives s(t) and another unique compilation of multipath jamming, $n_2(t)$, with uniform gain G_C. However, owing to the large magnitude of the jamming source, $n_2(t) >> s(t)$. Therefore, the total signal from the auxiliary antenna is thus defined by n(t), where

$$n(t) = G_C * (s(t) + n_2(t)) \cong G_C * n_2(t) \qquad (2)$$

Five Year Plan to Develop a Multichannel Optical Processor				
FY89	FY90	FY91	FY92	FY93
Phase I Development		Phase II Development		Phase III Development
Design, Build, and Test Single Channel Processor		Design and Build Multichannel Processor		Test and Evaluate Multichannel Processor

Figure 1: Diagram of the five year plan to develop an in-house multichannel optical processor.

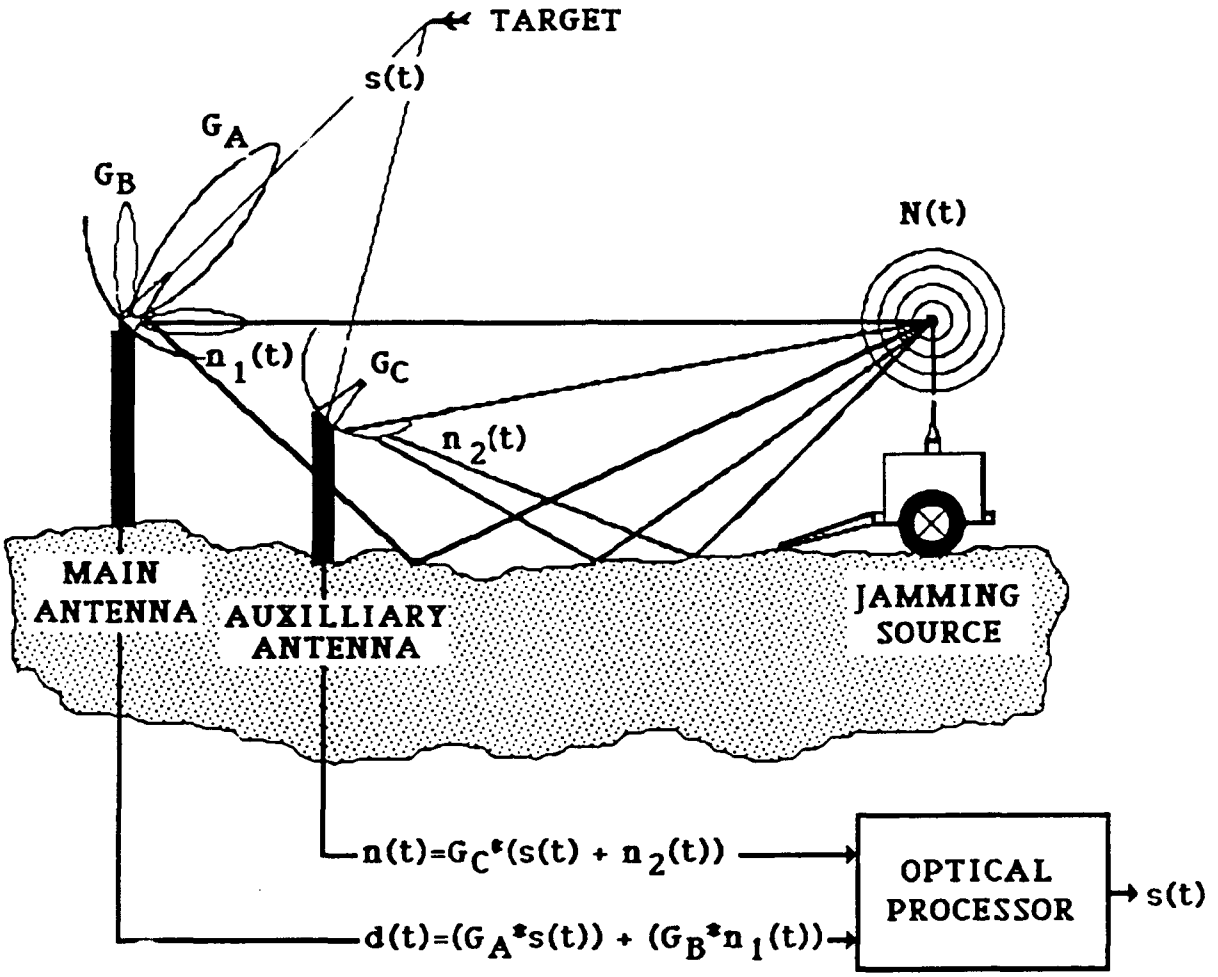

Figure 2: Scenario for adaptive optical processor. Main antenna receives target and multipath jamming signal. The jamming signal is coupled into the side lobe of the main antenna and thus receives less gain than the main signal, $G_A >> G_B$. An omnidirectional auxilliary antenna receives both target and multipath jamming signal with uniform gain. It is assumed that the jamming signal is much greater in magnitude than the target signal.

These two input signals, d(t) and n(t), are provided to the signal processor. Having been provided with these two input signals, d(t) and n(t), the signal processor must use n(t) to form an estimate to $n_1(t)$ and subtract this estimate from d(t). Call the estimate y(t) and define an error signal E(t), where

$$E(t) = d(t) - y(t) \qquad (3)$$

As the expected value of the squared error is minimized, E(t) will approach the value of the desired target signal, s(t).

2.2 Overview of Optical System The adaptive optical processor is based on the steepest descent algorithm and consists of two unique optical subsystems linked by a microcomputer as shown in the block diagram of Figure 3. The first subsystem performs an optical correlation between the signals d(t) and n(t). The signal from the auxiliary antenna, n(t), is used as a reference signal to determine the time delays of the multipath jamming signal, $n_1(t)$. The microcomputer collects and evaluates the correlation data and inputs corresponding delay and amplitude data to the second subsystem. The second subsystem uses this data to selectively weight the corresponding delays on an optically tapped acousto-optic delay line. A spatial integration of these tapped delays forms the estimate, y(t). The estimate is subtracted from d(t), thereby forming the error signal which is fed to the first subsystem where it is again correlated with n(t). This correlation result is used to update the taps applied to the acousto-optic delay line. These iterations will continue until the error signal has been minimized to within tolerance. The algorithm, computer programs, and optical architectures used to perform this adaptive optical processing task are described in detail in the next two sections.

3. Algorithm Considerations

3.1 Theoretical Application. As described in the previous section, the adaptive processing can be viewed as a minimizing problem, where the expected value of the squared error function, E(t), is the quantity to be minimized. As this approaches the minimum value, the estimate y(t) approaches the value of the multipath signal, $n_1(t)$. The estimate to the multipath can be described as a weighted sum of the various delays, τ_i, of the reference signal. The estimate can be expressed in continuous form, however, the discrete form is representative of the limitations in the optical system. We have

$$y(t) = \sum_{i=1}^{N} w_i(t) * n(t-\tau_i) \qquad (4)$$

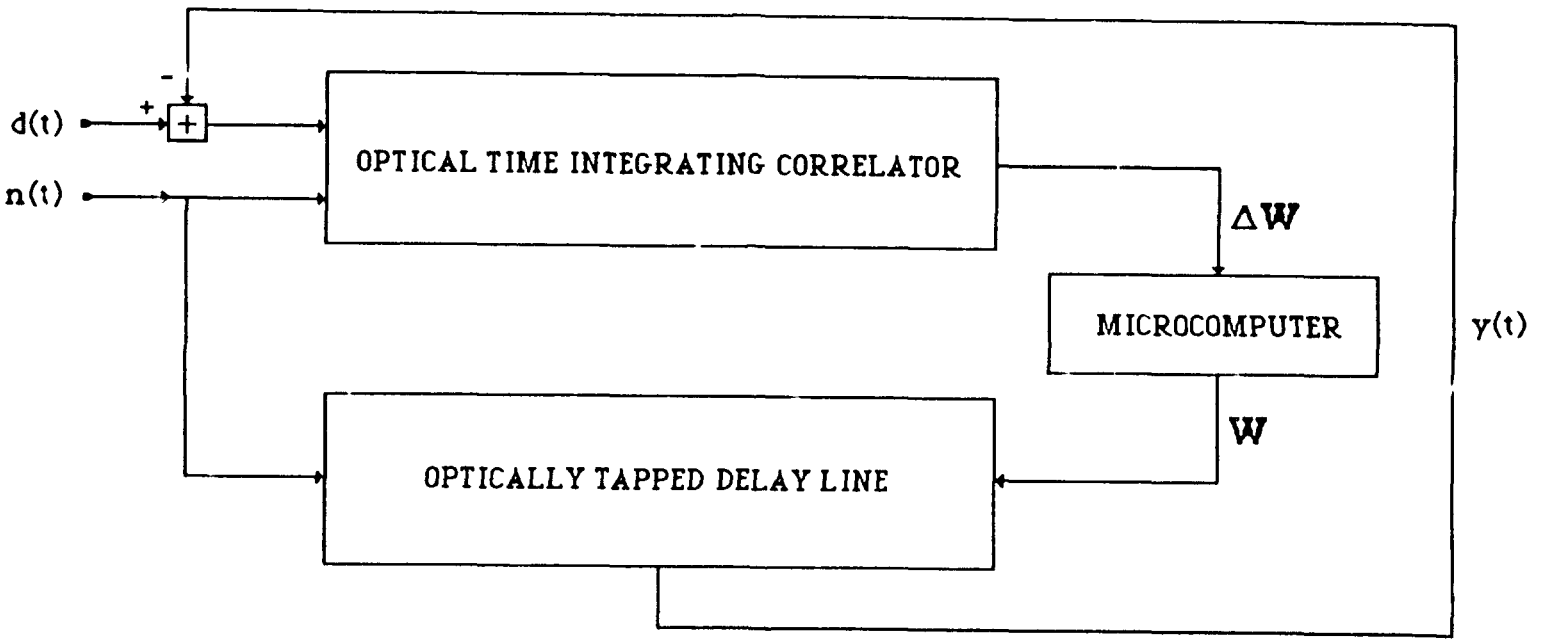

Figure 3: Block diagram of optical system.

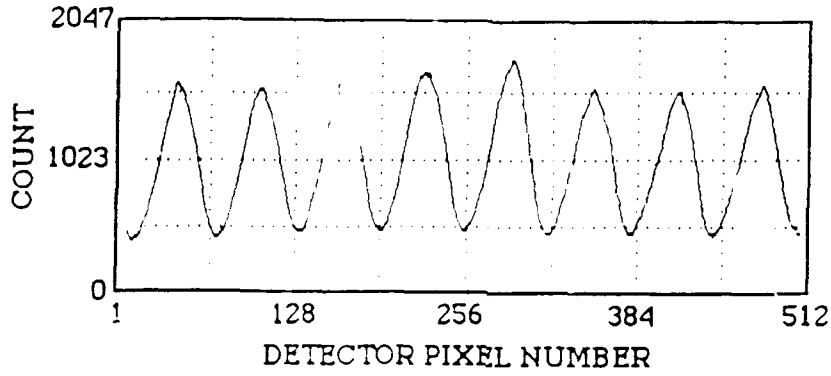

Figure 4a: Linear detector output from time integrating correlator. Demonstrates a positive correlation between two 2.75 MHz sinusoidal signals which are in phase with each other. Note the positions of the correlation peaks.

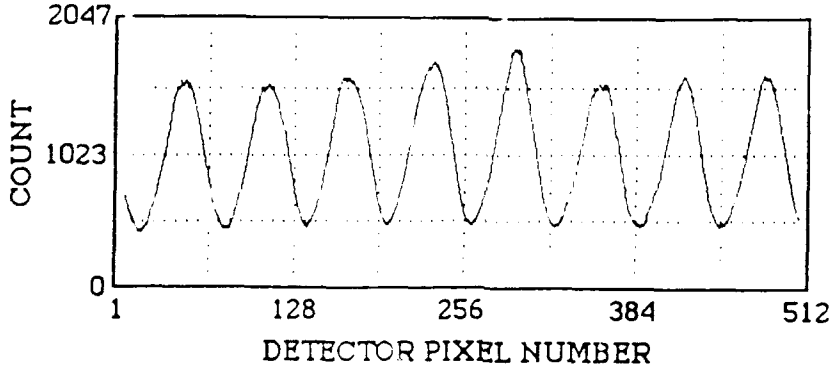

Figure 4b: Linear detector output from time integrating correlator. Demonstrates a positive correlation between two 2.75 MHz sinusoidal signals, where one signal is delayed by 36 degrees with respect to the other. Note how the positions of the correlation peak have shifted relative to their positions in Figure 4a.

where N is the total number of vector components which the optical system can compute, and the weights w_i are described by the correlation between E(t) and n(t)

$$w_i(t) = \int_0^T E(t) * n(t-T)\ dT \qquad (5)$$

where T is a dummy integration variable, and T is the processing time. The new error signal may be expressed as

$$E(t) = d(t) - \sum_{i=1}^{N} w_i(t)* n(t-\tau_i) \qquad (6)$$

The key is to find the optimum value of the weight vector, $\mathbf{W} = (w_1,...,w_i)$, so that E(t) is minimized.

The steepest descent algorithm is an iterative method for finding an optimum solution for cancelling the multiple delays present in a jamming signal. This method is summarized as follows:

$$\text{new } \mathbf{W} = \text{old } \mathbf{W} + \text{stepsize} * (\Delta\mathbf{W}) \qquad (7)$$

where $\Delta\mathbf{W}$ is a vector update and stepsize is a parameter to control convergence. The values for $\Delta\mathbf{W}$ are found by correlating E(t) and n(t) as described above. This approach is advantageous because it provides a global minimum and multiple delays are estimated as quickly as a single delay.[2,3]

However, there are also disadvantages. A large number of taps, corresponding to the size of the weight vector, is required to ensure accuracy. Convergence time is a function of the number of taps, which suggests a trade-off between accuracy and speed. Finally, the algorithm performance is limited by the precision of estimating the delays and forming the weight updates. If the estimated delays do not coincide with the actual delays, τ_i, then this approach will not converge to a solution. This limitation is a function of the optical and electronic hardware used to implement the algorithm.

3.2 Actual Application. In practice, the engineering implementation of this algorithm is not as straightforward as the mathematics suggests. To demonstrate the hardware limitations encountered when computing the optical correlation described mathematically in (5), consider the example shown in Figure 4a, where

$$s(t)=SIN(2\pi t/0.400\mu sec),$$

$$n_1(t)=n_2(t)=SIN(2\pi t/0.364\mu sec).$$

This correlation was performed optically between $s(t)+n_1(t)$ and $n_2(t)$. The architecture used to calculate this result is discussed in section 4. This figure displays a 3.2 μsec window with 6.25 nsec/pixel. The vertical axis represents the magnitude of the weight update ΔW, after integrating over 4 msec. Now permit a delay of 0.0364 μsec to be inserted in the multipath signal received by the main antenna, that is

$$n_1(t)=SIN((2\pi t/0.364\ \mu sec)+(2\pi*0.0364\ \mu sec/0.364\ \mu sec)).$$

$n_2(t)$ and $s(t)$ remain unchanged. The optically calculated correlation is shown in Figure 4b. Note that the correlation peaks have changed their location in proportion to the multipath delay. The weight update value at a given delay is proportional to the correlation magnitude. These weights are then applied to the tapped delay line, whose output is summed to form the estimate $y(t)$.

In actual system operation, however, the shift in peak location as a function of delay is not a constant. For example, if a delay of 30 degrees causes a shift in peak location by 20 units for one sample, and the same delay causes a shift of 10 units in a second sample, the system will not be able to use the correlation data to form accurate estimates of the delayed signal. Such problems as discussed in Section 7.1.2 led us to consider using the system's microcomputer to correct for errors caused by the optical and electronic hardware.

3.2.1 Parabolic Interpolation. A parabolic interpolation algorithm was written in Turbo Pascal 4.0 and used on the microcomputer to address system inefficiencies. This algorithm is used for finding the minima of a nonlinear function and is described in detail in References 2 and 4. It is important to note that this computer resident algorithm differs significantly from the theoretical approach described above. In the case of steepest descent, the mean square error is the minimized function, and the correlation magnitude represents the amplitude of the weight update. However, in the case of parabolic interpolation and limited range stepping (see Section 3.2.2), the amplitude of the correlation result is the minimized function, and the weight updates are selected so as to bring the amplitude of the correlation peaks to zero.

Briefly, the program assumes that a single variable function will approximate a parabola in the vicinity of a minima. Hence, after evaluating a function at three values of the variable, the program fits a parabola to this data and "guesses" that the minimum of the function occurs at the variable value which corresponds to the minimum of the fitted parabola. The function is evaluated at this new variable value. If the new function value is less than one of the function values at the three previous points used, then the new variable value replaces one of the old. The process is repeated and a new parabola is fit to the new set of three data points. When two successive estimates of the minimum differ by less than a predetermined tolerance, the process stops. The variable value which corresponds to the smallest function value is assumed to be the minimum.

The function that this program minimizes is the magnitude of the correlation result, such as shown in Figures 4a and 4b. We call this magnitude the energy function. As implemented here, the program first minimizes the energy function by holding the amplitude variable constant and changing the delay variable. Having completed this, the program holds the delay variable constant and changes the amplitude variable. After finding a minimum with this algorithm, the program continuously collects correlation data and monitors the value of the energy function. If the energy function increases by more than a pre-defined threshold, the program begins to actively vary the delay and weight values until the minimum energy has been restored. Although the shift in correlation peaks location is not a constant function of the delay, the peak shift is used to give the program a range from which to estimate delays..

In practice, parabolic interpolation was prone to finding local minima rather than the global minimum. To offset this problem, a user activated procedure was written to "kick" the program from the local minimum and allow it to find a new minima, which hopefully is the global minimum. The parabolic interpolation algorithm was found to be oversensitive to system noise. An error in the energy level could send the program searching for a minimum within a limited range which did not contain the global minimum. These shortcomings in using the parabolic interpolation algorithm led to the development of a more robust program.

3.2.2 Limited Range Stepping. This program was developed to address the problems we encountered in using the parabolic interpolation algorithm. As before, a range of variable values which might contain the global minimum is defined based on the amount of shift in the correlation peak. Correlation data is obtained and the energy function evaluated at five evenly spaced variable values within this range. The value which corresponds to the minimum energy is the starting point for the first step of the search routine. The range of variable values at which the energy function will be evaluated is restricted to a region about this new minimum.

The first step of the search routine incrementally increases the variable by a user defined step size. The energy function is evaluated at the new variable value. The program continues to change the variable until the energy function has been observed to increase at three consecutive settings. Then the program begins to incrementally decrease the variable until the error function increases at three consecutive settings. At this point the program further restricts the range, decreases the step size, and evaluates the energy function within this restricted range. The variable which corresponds to the minimum energy within this limited range is assumed to be the global minimum. Having found a minimum, similar to the previously described program, the energy function is continuously monitored.

This program searches a large range of variable values before limiting itself to looking for a minimum within a smaller range. This enables it to find the global minimum and ignore local minima almost every time. Additionally, this program demonstrated an ability to overcome problems related to system noise. For example, the magnitude of two consecutive correlation results might differ by as much as 5% due to noise in amplifiers, phase drift in the signal

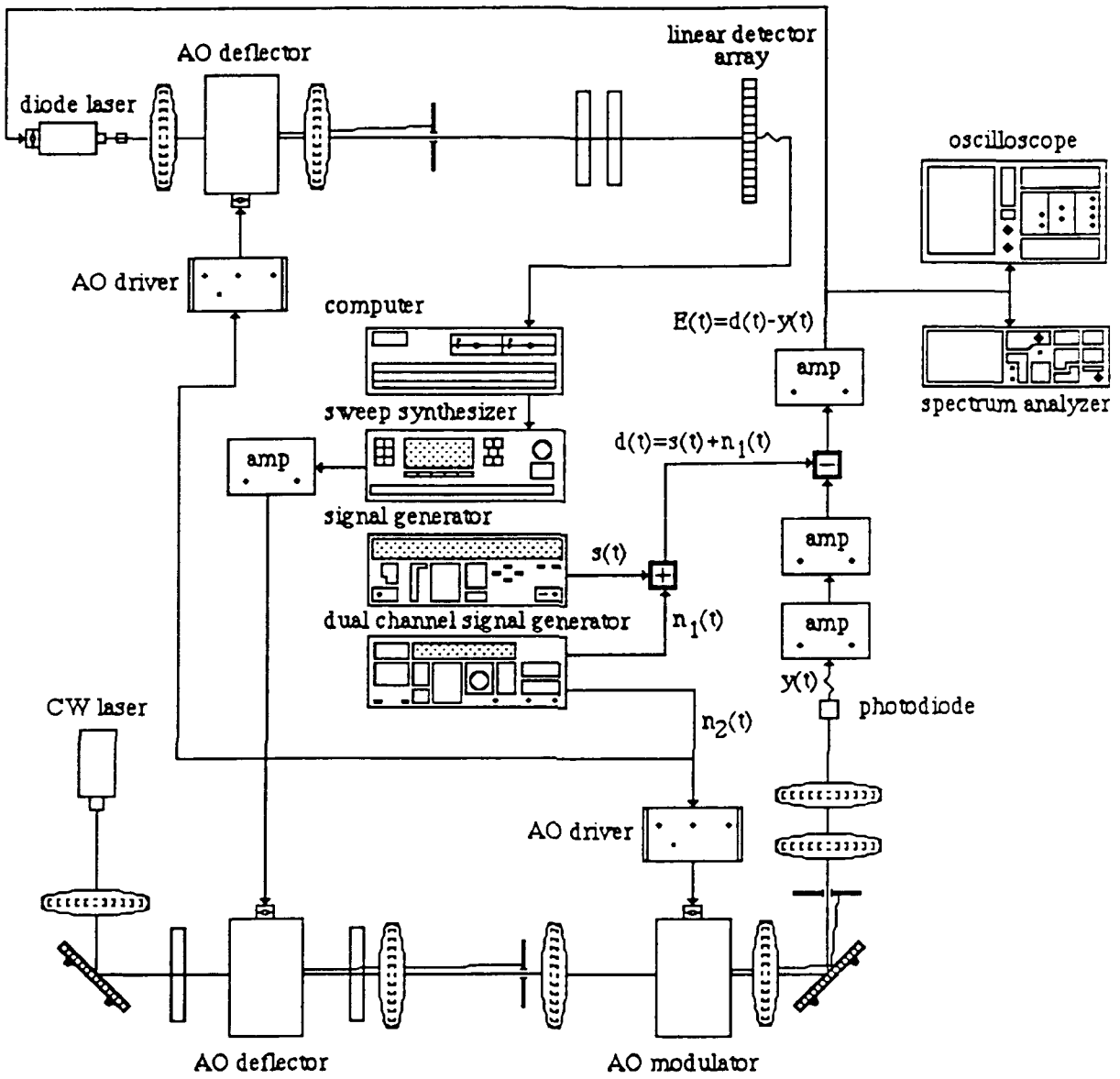

Figure 5: Architecture for single channel adaptive optical processor. The processor consists of two optical subsystems linked by a computer. The first subsystem, a time integrating correlator, performs an optical correlation between E(t) and $n_2(t)$. The computer extracts weight and delay information from this correlation result, sending it to the spatial light modulator (SLM) in the second optical subsystem, which is an optically tapped delay line. Here an acousto-optic (AO) deflector is used as an SLM to selectively tap various delays on an AO delay line. The sum of these weighted delays forms y(t), which is an estimate to the interference signal $n_1(t)$. Equipment details are to be found in the appendices.

generators, etc. However, the program will continue to increment the variable until the error function has been observed to increase at three consecutive variable settings. This condition appears to make the program largely insensitive to system noise.

3.2.3 Other Possible Approaches. Reference 2 contains descriptions of other possible approaches to overcome system hardware errors in implementing the steepest descent algorithm. These approaches include conjugate directions, simulated annealing, a neural network controller, or some combination of the above approaches. These programs will be examined further during Phase II of the in-house effort.

4. System Architecture

4.1 Time Integrating Optical Correlator. The first subsystem within the optical processor is the time integrating optical correlator[5,6]. The manufacturer names and model numbers of the equipment are listed in Appendix A. Detailed optical layouts are drawn in Appendix B. As shown in Figure 5, the input d(t)-y(t) modulates the output of a GaAlAs 670nm diode laser (3 mW power.) A 45^{O} line generating lens and a 150mm focal length plano-cylindrical lens collimate the output beam, shape it into a 1.5 mm x 22 mm line, and direct it at the Bragg angle to the input aperture of the acousto-optic modulator (AOM). The optical signal illuminates the entire 22 mm aperture of the deflector and thereby simultaneously interacts with a 5 μsec portion of the acoustic signal.

The auxilliary channel signal $n_2(t)$ modulates a 40 MHz carrier to form a double sideband modulation input to the AOM. When $n_2(t)$ is a 2 MHz sinusoid, the spectral content of the RF input to the AOM has components at 38 MHz, 40 MHz, and 42 MHz. The +1 diffracted order now consists of three unique optical frequencies, namely the optical frequency characteristic of the diode laser, f_{opt}, and the Bragg-shifted frequencies: f_{opt}+38 MHz and f_{opt}+42 MHz. The beams within the diffracted order are imaged onto a 512 element linear detector array, giving rise to a moving interference pattern which sweeps across the array. When the laser output modulated at n(t) correlates with this moving pattern, a non-zero correlation result is obtained, such as shown in Figure 4.

The linear detector array is mounted onto an evaluation board and is sampled at 12 bits. A custom interface board and a data acquisition board, which are mounted in a computer, collect and digitize the data from the detector array. The computer, using one of the approaches discussed in the previous section, selects the appropriate weights and delays corresponding to the correlation result. This data is then sent through a GPIB board to the spatial light modulator in the optically tapped time delay.

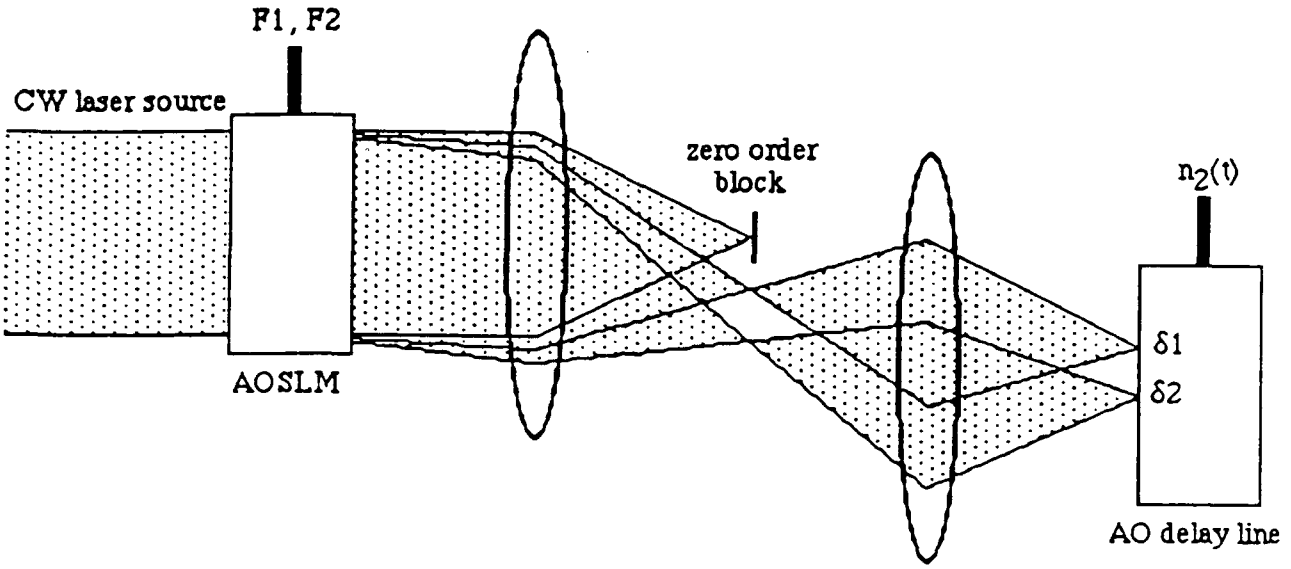

Figure 6: Acousto-optic spatial light modulator (AOSLM) selectively tapping two delays on an AO delay line. Each carrier frequency, F_i, input to the AOSLM corresponds to a unique tap postion, δ_i, at the delay line. The weight at a given tap position corresponds to the amplitude of the corresponding carrier frequency. See Appendix B for details of the optical layout.

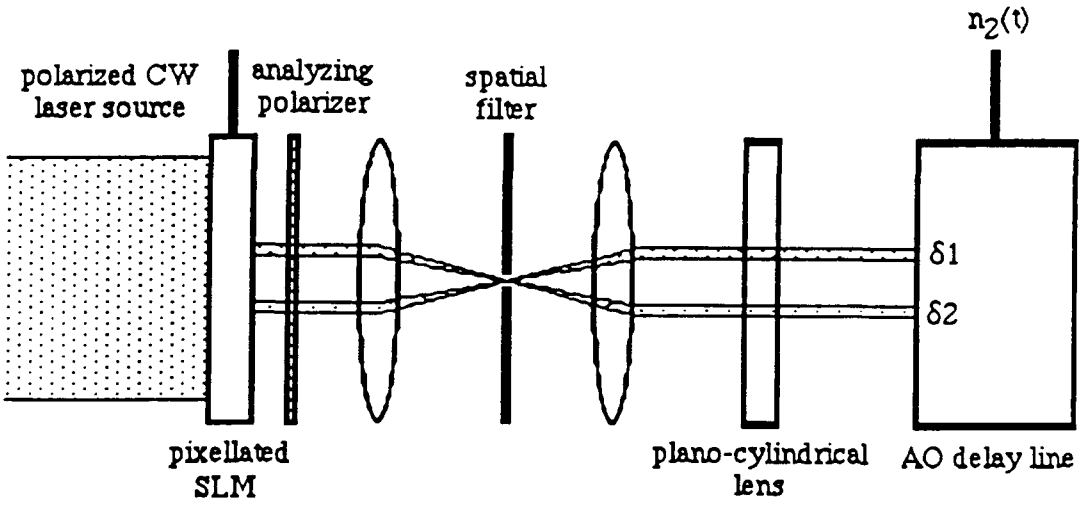

Figure 7: Apparatus used to permit a two-dimensional pixelated spatial light modulator (SLM) with binary transmission characteristics to perform as an enhanced dynamic range one-dimensional SLM. This SLM is used to tap an acousto-optic (AO) delay line.

4.2 Optically Tapped Time Delay. A 40 MHz AO deflector is used as a spatial light modulator (SLM) in the optically tapped time delay. By varying the carrier frequency and the RF power driving this device, the deflector performs as an SLM. The computer (via a GPIB board) controls the frequency and power output of a synthesized sweeper, which is amplified to drive the deflector cell. A CW input beam from a 531 nm frequency doubled diode-pumped YAG (25 mW power) fully illuminates the input aperture of the SLM. The optical system which follows the SLM is diagrammed in Appendix B. This optical system is designed to "magnify" the angular divergence of the +1 diffracted order and ensure that all beams within the +1 order emerge parallel to one another.

The light which is spatially modulated by the SLM is directed by these optics onto a 40 MHz AOM used as a delay line. The optically tapped and weighted delays are summed by a lens at the output of the delay line and the +1 diffracted order is focused onto the photodiode. The amplified output from the photodiode is the estimate to the jammer, y(t). The estimate is subtracted from the main antenna signal, d(t), amplified and sent to the first subsystem, thereby initiating the next iteration.

5. Selection of Spatial Light Modulator

5.1 Candidate Spatial Light Modulators. The spatial light modulator (SLM) is used to variably tap and weight an acousto-optic delay line. During the course of this project, three SLM devices were considered for this application: a liquid crystal display (LCD), a magneto-optic SLM (MOSLM), and an AO deflector used as an SLM (AOSLM). The use of these devices as SLMs is described briefly below, and in more detail in References 7, 8, and 9.

5.1.1 Acousto-optic Deflector Used as an SLM. Referring to Figure 6, the carrier frequency, F1, corresponds to the deflection angle for proper positioning of the probe beam onto the AOM. The carrier amplitude corresponds to weight, w_i, for each delayed signal. Multiple delays, δ_1 and δ_2, of function $n_2(t)$ are generated by feeding the deflector with multiple carriers, F1 and F2.

The multiple diffracted beams, corresponding to multiple delays, are not completely independent from one another. Each additional generated beam depletes the total optical power available to each of the other beams. In addition, intermodulation between multiple acoustic beams within the AO device further limit performance. These effects limit the AO deflector in the total number of simultaneous delays which it can address.

5.1.2 Pixellated SLMs. In addition to the AOSLM, two-dimensional pixellated devices are also candidates for this application. Referring to Figure 7, the horizontal dimension of the pixellated SLM is used to position the probe beam at the appropriate delays on the aperture of the AOM. For two-dimensional pixel grids, where each pixel is binary in amplitude, a plano-

Table I: Summary of SLM characteristics and system requirements

device	contrast ratio (dB)	system light efficiency (%)	number of grey levels	number of spatial weights	speed (KHz)
requirements	15.0	5.0	1000	100	0.10
LCD	9.2	0.4	162	162	0.06
MOSLM	9.7	0.2	256 [a]	256 [a]	0.12
AOSLM	14.5	77.6	1000	100 [b]	200.0

[a] This is calculated for a 256 x 256 device.
[b] Theoretical limit based on the time bandwidth product of AO deflector.

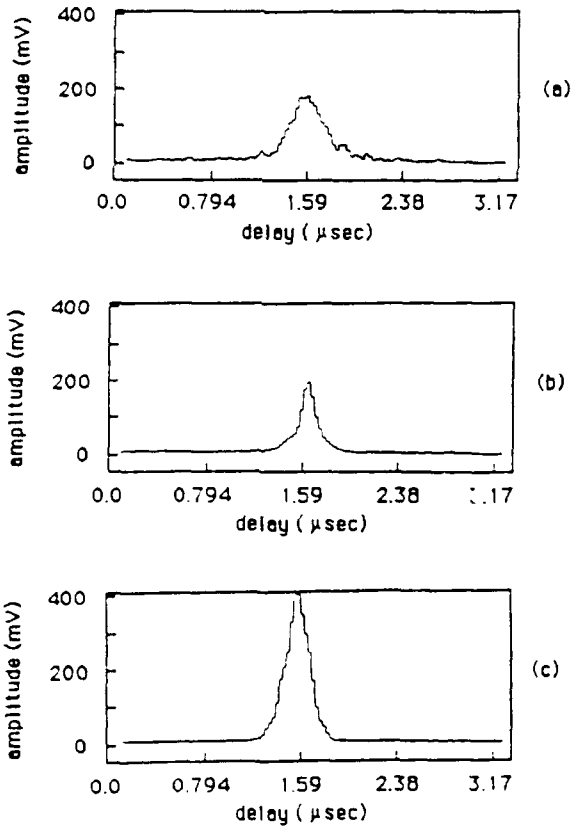

Figure 8: Spatial intensity profiles of candidate spatial light modulators (SLMs). (a) Liquid Crystal Display; (b) Magneto-optic SLM; (c) Acousto-optic SLM.

cylindrical lens can be used to sum the number of "on" pixels at a given column location to provide the proper amplitude weights, w_i [10]. However, if each pixel were capable of generating a sufficient number of grey levels, then a single pixel might be used to appropriately weight the selected delay. Due to the pixellated structure of the SLM, strong diffraction about the pixel grid becomes system noise which must be removed. As shown in Figure 7, this is accomplished with a spatial filter.

5.2 Spatial Light Modulator Requirements. A comparison was made of each device to determine how well it matched SLM requirements, which in turn were determined by overall system performance specifications. We find that the LCD and MOSLM fall far short of the required contrast ratio and system light efficiency. The AOSLM meets or exceeds system specifications for system light efficiency, number of grey levels, spatial resolution, speed, and is 0.5 dB down from the required contrast ratio. Of the devices tested here, the AOSLM provides the best performance characteristics for an operable electro-optic multipath delay estimation architecture.

5.2.1 Contrast Ratio. This parameter is perhaps the most critical SLM characteristic for this system application. It is essential that the SLM output places light at precise locations along the input aperture of the delay line. For example, consider the case of a single delay of arbitrary weight. Suppose this delay is at 1.0 μsec from the transducer of the AO modulator. The width of the probe beam at this delay location will determine the accuracy with which the estimate y(t) can be formed. Additionally, if stray light leaks through the SLM and is imaged onto the delay line at delays different from 1.0 μsec, the system will falsely interpret this light as another weighted delay. Computer simulations were performed to determine the effects of poor contrast ratio on the systems ability to cancel unwanted jamming signals.[1] It was found that the system would not iterate to a solution with light leakage of more than a few percent. Therefore, it was determined that a minimum contrast ratio of 15 dB is required.

To measure contrast ratio, a linear detector array replaced the AO delay line. The SLM output was focused onto the detector array. The output of this detector array, viewed on an oscilloscope, provided a measure of the spatial intensity profile of the SLM output. Contrast ratio is defined here as the ratio of peak amplitude of the SLM's output intensity profile to the RMS of the intensity outside the 3 dB range of this peak. The spatial intensity profiles of the candidate SLMs are shown in Figure 8, the measured contrast ratios listed in Table I.

5.2.2 System Light Efficiency. System light efficiency is defined here as the ratio of light intensity before the SLM to the light intensity at the delay line. The required system light efficiency depends on the maximum power of the laser source and the efficiency of the photodiode. To ensure system portability, a small laser with less than 20 mW of power is used. The output of the detector must produce at least 10 mV peak-to peak voltage to overcome other system noise. Using these criteria, a minimum system light efficiency of 5% is necessary.

Unlike many reported transmission measurements, which report single pixel throughput, we are interested in the transmission through a large region of pixels. In measuring the SLM's system light efficiency, we also take into account the transmission through any polarizers, optics, or filters necessary to achieve maximum contrast ratio. For example, consider the measurement apparatus sketched in Figure 7.

Polarized, collimated light is incident onto the SLM. The SLM rotates the input polarization according to the input signal. The light which passes through the SLM is then analyzed by a linear polarizer. Due to the pixellated structure of the SLM, strong diffraction about the grid occurs. This diffracted light is removed by placing a spatial filter in the Fourier plane of a biconvex lens, allowing only the DC component to pass. A second biconvex lens recollimates the light after the spatial filter.

At this point, the beam has a circular cross section. If this beam were to be focused by a plano-cylindrical optic, the circular cross section would produce a non-uniform spatial intensity profile at the focal plane. That is, one would find more light about the optical axis than in the adjacent regions. To counter this effect, the beam must be given a rectangular cross section. This is accomplished by placing a rectangular aperture in the path of the collimated beam, prior to the plano-cylindrical lens. Each component in this optical set-up is necessary for the SLM to provide a maximum contrast ratio. Hence, the entire SLM system is considered to include the SLM device as well as all associated optics and filters.

It must be noted here that the system light efficiency measurements listed in Table I were taken under conditions to ensure maximum system throughput for each candidate SLM. For the pixellated devices, this entailed placing all pixels in the transmissive, "on" position. In a typical operating scenario, it is unlikely that all pixels will be "on" simultaneously. For example, in the case of a single delay, only a single pixel column would be "on", the rest of the pixels would block light, thereby reducing the system light efficiency below the values recorded in Table I. Similarly, the AOSLM was measured for maximum diffraction efficiency, i.e. when only a single carrier frequency is driving the cell. However, in a case where there are multiple delays, the amount of light available to any single delay would be depleted by each of the other delays.

5.2.3 Number of Grey Levels. The number of grey levels is the maximum number of unique amplitude weights which can be applied to a given delay, which determines the precision with which the SLM may reproduce a weight vector. At least 1000 different weights is required to meet system performance criteria.[1] For SLMs with binary pixels (only "on" and "off") the number of pixels in a column determines the number of grey levels. However, if the individual pixels have a gray scale capability then the dynamic range would be the number of distinct levels in the gray scale multiplied by the number of pixels in the column. Figure 7 shows a vertical column of pixels on the SLM being summed by a plano-cylindrical lens to form a weighted delay. For the AOSLM, the dynamic range is a function of the range of amplitudes of the carrier frequency used to drive the deflector cell. This is then a function of the dynamic range of the signal generator

to drive the deflector cell. This is then a function of the dynamic range of the signal generator driving the AOSLM.

5.2.4 Number of Spatial Weights. The number of spatial weights is the number of delays achievable with the SLM. At least 100 unique delays are necessary to meet system performance criteria.[1] For the pixelated SLMs, the number of pixels in a row determines the number of spatial weights possible with the device. For the AOSLM, the number of spatial weights is a function of the time-bandwidth product of the cell. For the 40 MHz deflector cell the time aperture is 5 μsec and the bandwidth is 20 MHz which produces 100 resolvable spatial weights. For the 70 MHz deflector cell the time aperture is 10 μsec and the bandwidth is 40 MHz which produces 400 resolvable spatial weights.

5.2.5 Speed. The speed is defined as the time it takes to reconfigure the SLM for a new update to the signal estimation. The pixellated SLMs have a maximum speed or frame rate specified by the manufacturer. For the AOSLM, the speed is a function the time aperture of the device. For example, the 40 MHz deflector has a time aperture of 5 μsec. The speed is 1/5 μsec or 200 kHz.

6. System Tests and Results

6.1 Critical Test Parameters. The goal of the Phase I development was to provide substantial proof of the concept that the electro-optic architecture described herein is a good candidate for meeting USAF needs in the adaptive signal processing of multipath interference signals. A list of "critical test parameters" was drawn up for the Phase I system to measure progress toward this goal. If the system could perform at the level defined by these parameters, then we would have sufficient confidence in this approach to warrant further development. These critical test parameters are listed below, followed by a report as to how the system measured up to each parameter:

(i) Demonstrate the ability of the AOSLM to select and weight delays on the acousto-optic delay line.
(ii) Demonstrate the ability of the optical processor to achieve a 30 dB cancellation of a monotone, single delay signal over a full range of delays.
(iii) Demonstrate the ability of the optical processor to achieve a 30 dB cancellation of a monotone, single delay signal while operating as a closed loop system (ie. no user interaction.)

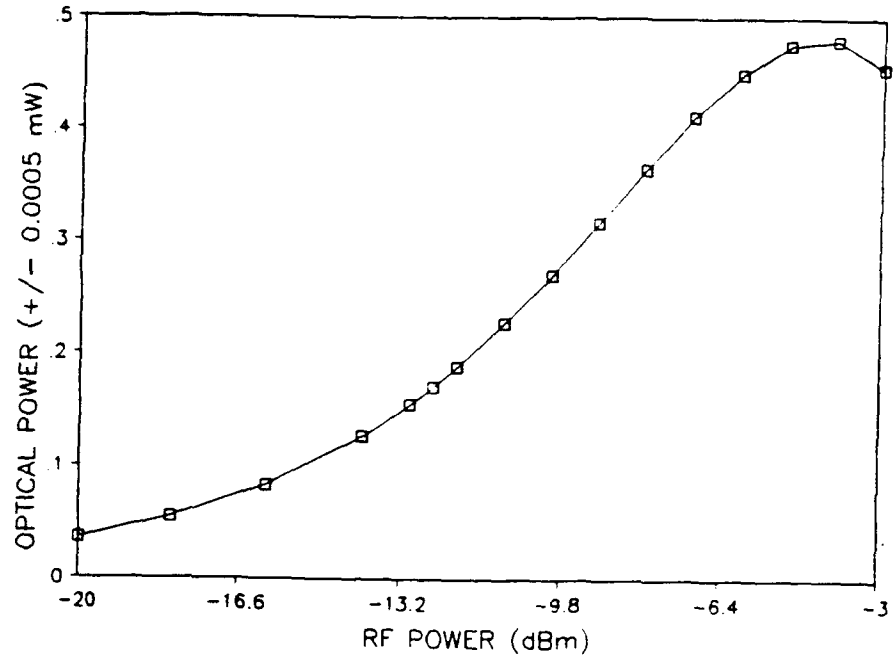

Figure 9: Optical power in the +1 diffracted order of the acousto-optic spatial light modulator (AOSLM) as a function of input RF power. This demonstrates the ability of the AOSLM to tap the delay line with weights having a 30 dB dynamic range.

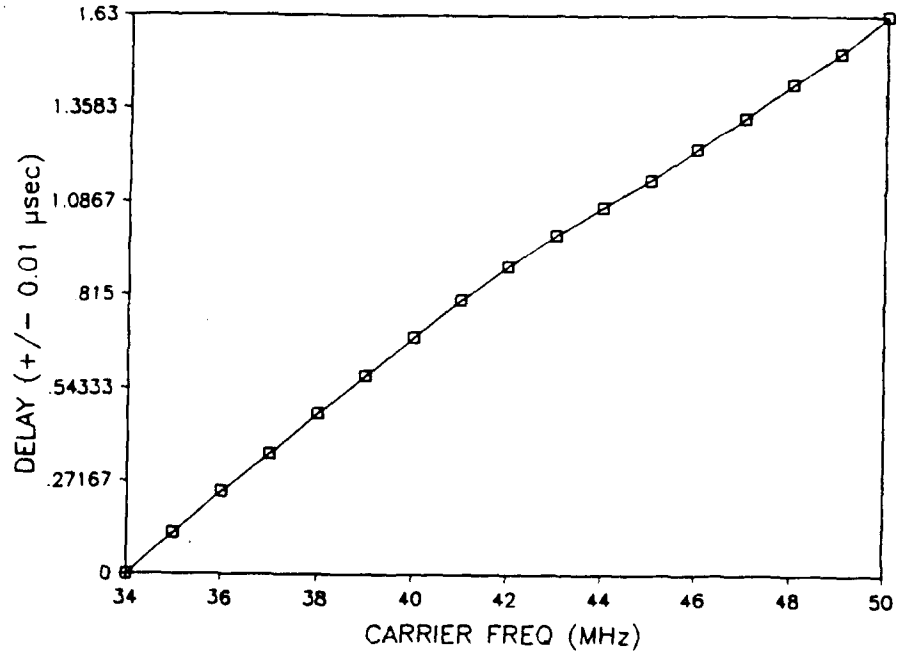

Figure 10: Delay of signal at output of the optically tapped delay line as a function of the carrier frequency input to the acousto-optic spatial light modulator (AOSLM). This demonstrates the ability of the AOSLM to tap 1.6 µsec of delay. A greater range of delay could be accessed by appropriate changes in the imaging optics.

(iv) Demonstrate the ability of the closed loop system to dynamically achieve a 30 dB cancellation of a monotone, single delay signal as the delay varies with time.

6.2 System Performance Measurements.

6.2.1 Demonstration of AOSLM's Ability to Select and Weight Delays.

Experimental tests of the AOSLM's ability to vary both amplitude and delay were performed. The first test examined the dynamic range of the amplitude (also termed "grey level" in this report for purposes of comparison with pixellated devices) as a function of RF power applied to the AOSLM. This measurement was performed by replacing the photodiode in the space integrating correlator with an optical power detector. The RF power driving the AOSLM is generated by the synthesized sweeper followed by a 37 dB amplifier. As the RF output power of the sweeper is varied over the range of -20.00 dBm to -3.00 dBm, the optical power is monitored. The results are displayed in Figure 9.

A curve fit to the data over the range of -16.00 dBm to -5.00 dBm reveals that a linear fit models the data with a correlation coefficient of 0.993. Since the sweeper has an effective amplitude resolution of 0.01 dBm, there are approximately 1100 unique "grey levels" within the linear range of the amplitude/RF power curve.

The ability of the AOSLM to vary the spatial location of a focused beam incident on the AO delay line is also of interest. Measurement of the delay as a function of carrier frequency driving the AOSLM was performed. The photodiode output in the space integrating correlator was observed on an oscilloscope. A 2 MHz monotone signal amplitude modulated the 40 MHz carrier on the AO delay line. The carrier frequency applied to the AOSLM was varied over the range of 34 MHz to 50 MHz, causing the diffracted beam to sweep across the input aperture to the AO delay line. The resultant shift in delay, as observed on the oscilloscope, is recorded in Figure 10.

A curve fit to the entire displayed data range shows that a linear fit models the data with a correlation coefficient of 0.998. The effective frequency resolution of the sweeper is 0.1 MHz. Hence, within the 20 MHz bandwidth of the AOSLM, we can easily achieve the theoretical limit of 100 unique spatial weights (ie., delays) with this configuration.

The Turbo Pascal program which extracts information from the optically computed correlation is capable of varying both the amplitude and carrier frequency applied to the AOSLM via a GPIB interface.

6.2.2 Demonstration of 30 dB Cancellation of Single Delay. Having found and characterized an SLM suitable for this application, the next goal was to demonstrate the ability of the optical system to form a 30 dB cancellation of a monotone, single delay interference signal. This was performed with the test apparatus shown in Figure 11. A test signal s(t), a sinusoid with frequency 2.75 MHz, is added to an interference signal $n_1(t)$, a sinusoid with frequency 2.50 MHz. The 40 MHz carrier on the AO delay line is amplitude modulated by $n_2(t)$, where $n_2(t)=n_1(t+\tau)$ for

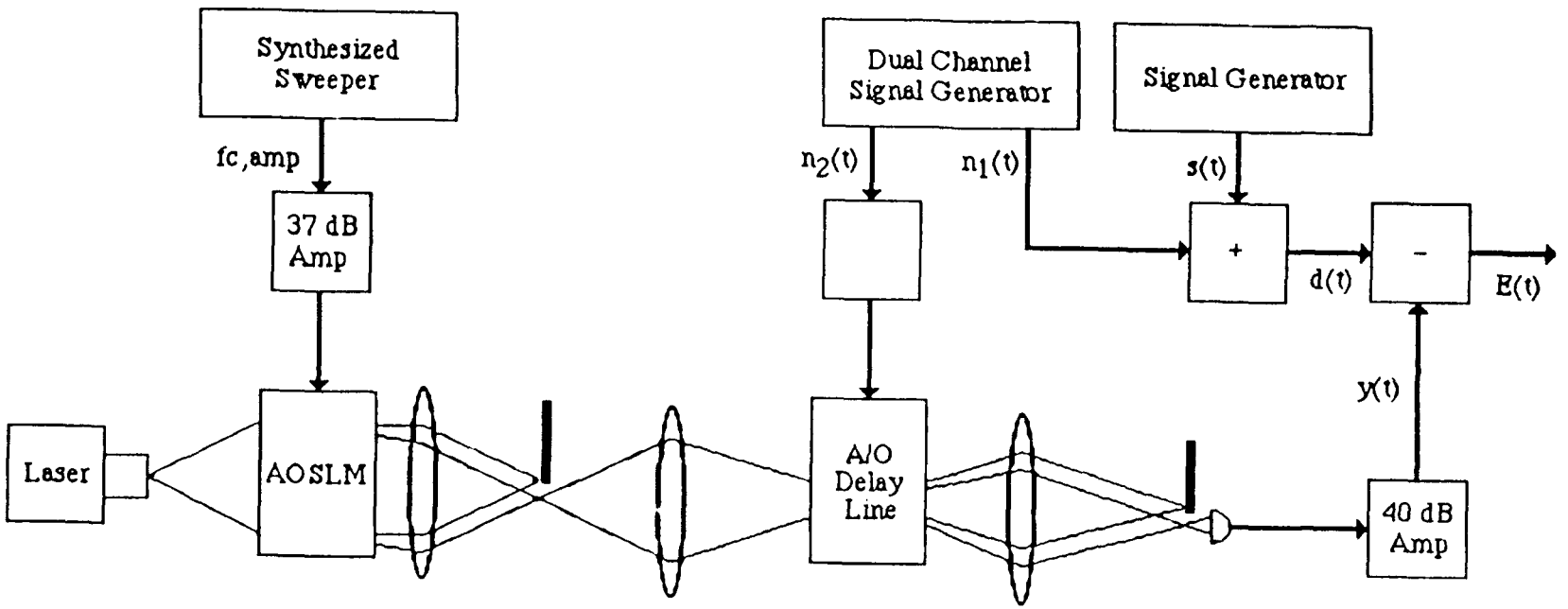

Figure 11: Block diagram of test apparatus used to measure the single delay cancellation capability of the optically apped delay line. See Appendix B for details of the optical layout.

some arbitrary time delay, τ. A single probe beam, corresponding to a single delay is incident onto the delay line. The intensity and spatial location of this probe beam are selected by manually adjusting the carrier frequency and amplitude of the RF signal driving the AOSLM. The probe beam taps a delay of $n_2(t)$ at the AO delay line and the light collected at the photodiode represents the estimate, y(t), to the interference signal, $n_1(t)$. The estimate y(t) is subtracted from d(t), the output being equal to E(t), the error signal. E(t) is observed with a spectrum analyzer. The sweeper output is manually adjusted so as to minimize E(t).

A plot of the spectrum analyzer output is displayed in Figure 12a. This plot represents the 2.50 MHz single tone jamming signal ($n_1(t)$) masking a 2.75 MHz single tone signal of interest (s(t)). y(t)=0 in this plot. The magnitude of $n_1(t)$ is -6.8 +/- 0.1 dBm. Now y(t) is manually adjusted by varying the signal driving the AOSLM so as to minimize E(t). Figure 12b shows this result, demonstrating a 35 +/- 5 dB cancellation of the interference signal. A similar measurement is made over a full 2π range of delays, ie. t=0 to 0.4 μsec. The mean cancellation ratio over this range is 30.2 +/- 3.9 dB. This satisfies the cancellation ratio goal of 30 dB. The reason for the large uncertainty in this measurement is discussed in Section 7.1.3.

6.2.3 Demonstration of Closed Loop Performance. The next step was to demonstrate the ability of the optical processor to achieve a 30 dB cancellation of a monotone, single delay interference signal while operating as a closed loop system. In the previous test, a 30 dB cancellation ratio was achieved by manually selecting the delays and weights on the AO delay line. This measured the ultimate ability of the optical system to cancel the test signal. However, with the processor operating as a closed loop system the delays and weights are selected by the processor itself. The Turbo Pascal program resident in the computer extracts the delay and weight information from the correlation result, which in turn is updated by a feedback loop from the space integrating correlator.

The apparatus used for this test is shown in Figure 5. The same test signals used in the previous section are also used here, namely: s(t) is a 2.75 MHz sinusoid, $n_1(t)$ is a 2.50 MHz sinusoid, $n_2(t)=n_1(t+\tau)$. When these test signal are applied to the system, the linear detector array shows a positive correlation between E(t) and $n_2(t)$. The computer notes the location and amplitude of the correlation peaks and makes several "guesses" at the proper delay and weight which will minimize the amplitude of the correlation peaks. These guesses are made in accordance with the computer algorithms discussed in Section 3.

The synthesized sweeper changes the frequency and amplitude of the signal driving the AOSLM. With these inputs, the AOSLM adjusts the location and intensity of the probe beam on the AO delay line. The photodiode collects the optical signal from the tapped delay line, and the photodiode output is subtracted from d(t), thereby forming a new value for E(t).

E(t) modulates the diode laser which feeds the optical signal into the time integrating correlator, so that a new value for E(t) changes the amplitude of the correlation result. The computer takes note of this result and revises its next guess accordingly. The system will actively

a.

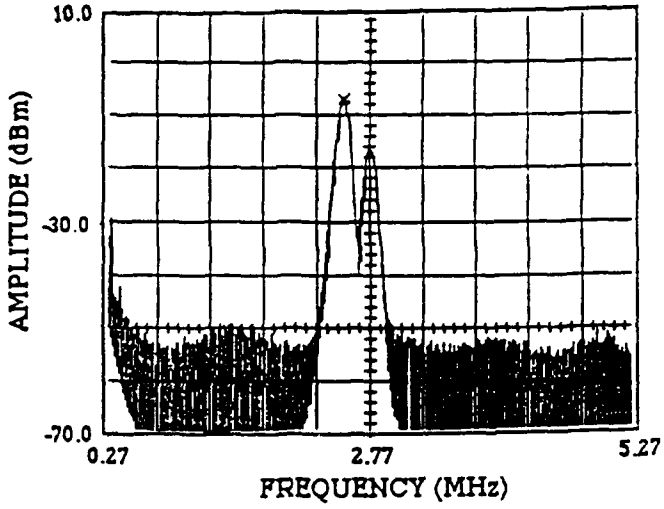

b.

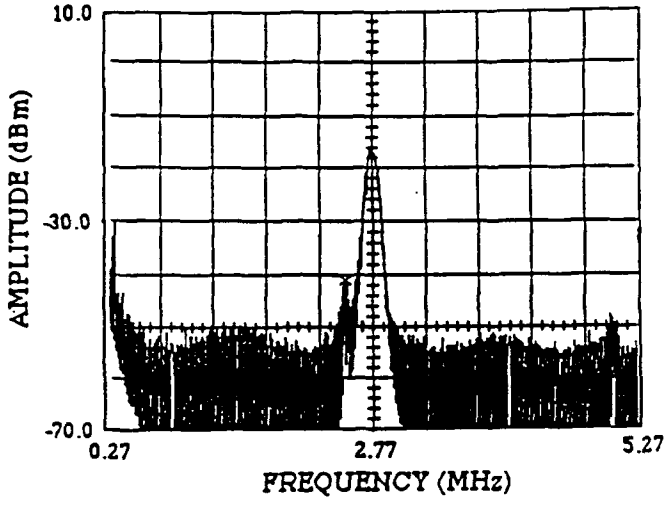

c.

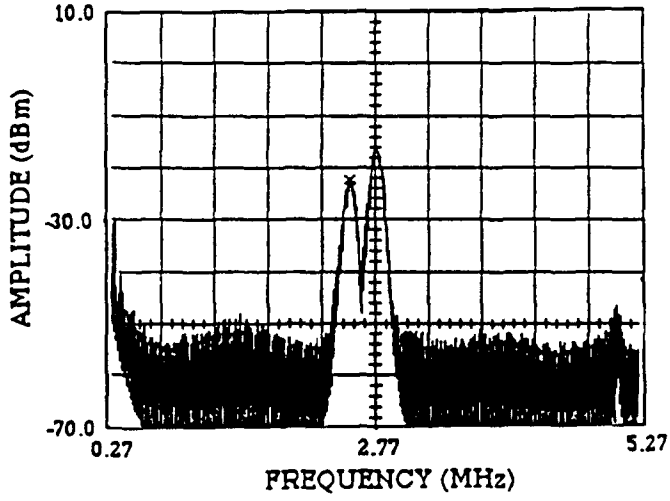

Figure 12: Signal spectra of (a) a 2.75 MHz signal masked by a 2.50 MHz interference signal: (b) 35 dB cancellation of interference signal achieved by manually selecting the proper weights and delays on the optically tapped delay line; (c) 15 dB cancellation of interference signal achieved by closed loop (ie., no user interaction) optical processor.

search the solution space until the amplitude of the correlation result has been reduced below a preset tolerance.

In practice, the system finds a minima of E(t) within several dozen iterations. A typical closed loop cancellation result is shown in Figure 12c. Note that this represents a cancellation of only 15.7 +/- 0.5 dB. The goal was for the system to achieve a 30 dB cancellation. Our evaluation of this result is deferred to Section 7.1.1.

6.2.4 Demonstration of Adaptive Cancellation. The next goal was to demonstrate the ability of the optical processor to adaptively cancel a dynamically varying time delay, simulating a change in the multipath environment. The system should be able to provide the performance described in Section 4.1.3 while the delay τ is being changed. To test this, the delay of $n_2(t)$ was manually varied over a full 2π range. At each delay setting, the optical processor was given enough time to cancel the new delay of $n_2(t)$ before the next delay was entered. The magnitude of $n_1(t)$ is -6.8 +/- 0.1 dBm. This data is recorded in Table II. The mean cancellation of $n_1(t)$ over this range of delays is 15.2+/- 2.4 dB.

7. Analysis and Conclusions

7.1 Analysis of System Performance.

7.1.1 Cancelling Limitation of Closed Loop System. We have demonstrated that the optical processor is able to provide 15.2 +/- 2.4 dB adaptive cancellation of a monotone, single delay test signal. However, manual adjustment of the position and amplitude of the optical tap on the delay line in an open loop system allowed for cancellation of 30.2 +/- 3.9 dB using the same test signals. The dynamic range of the diode laser in the time integrating correlator proves to be a major factor in the inability of the closed loop system to realize the performance of the open loop system. While observing E(t) on the oscilloscope depicted in Figure 5, we manually vary the position and amplitude of the optical tap to the optimal settings to minimize the amplitude of E(t).

When the closed loop system operates, the computer determines if it has reached a minimum by measuring the amplitude of correlation peaks (shown in Figure 4) as gathered by the linear detector array. Unfortunately, the amplitude of the correlation peaks is a function of the modulation depth of the diode laser which illuminates the AO deflector. From Equation 3, when $s(t)=0$, we have

$$E(t) = d(t) - y(t) = s(t) + (n_1(t) - y(t)) = n_1(t) - y(t) \qquad (8)$$

This expression is correlated with $n_2(t)$ in the interaction between the modulated laser light and the AO device. As the estimate, y(t), approaches $n_1(t)$, the amplitude of E(t) grows smaller. We have

Table II: Adaptive cancellation performance of optical processor

delay (deg)	delay (msec)	amplitude of cancelled signal (dBm)
-180	-0.200	-25.0 +/- 3.0
-120	-0.133	-15.0 +/- 1.0
-60	-0.066	-22.0 +/- 1.5
0	+0.000	-27.0 +/- 2.0
+60	+0.066	-25.0 +/- 2.0
+120	+0.133	-25.0 +/- 2.0
+180	+0.200	-15.5 +/- 1.0

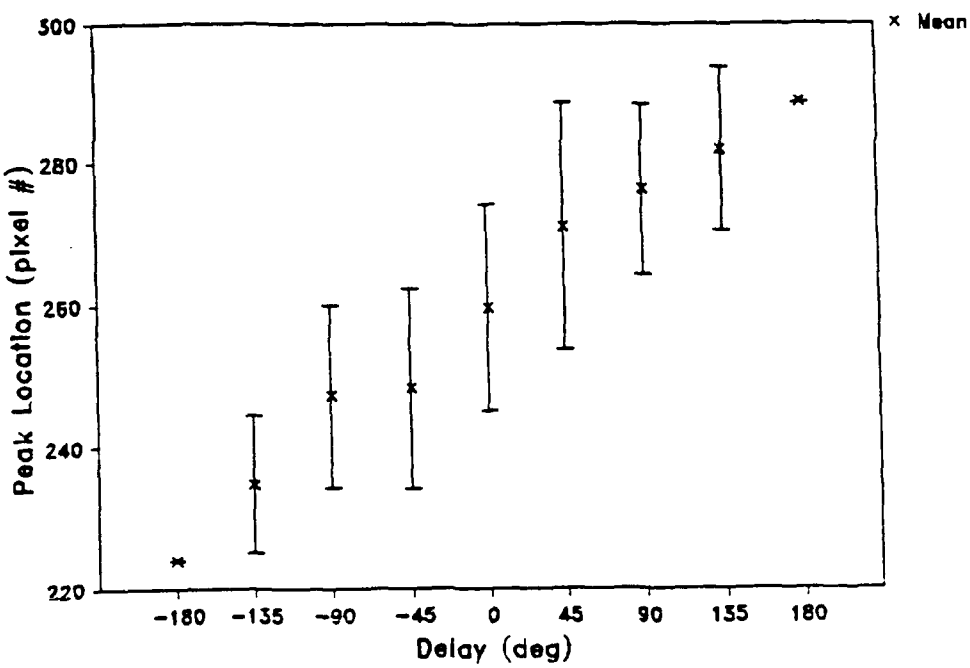

Figure 13: Location of correlation peak at linear detector array as a function of delay between d(t)-y(t) and n(t). The error bars represent two standard deviations about the mean for the collected data. This demonstrates an inability to consistently predict a fixed correlation peak location for a given delay when $y(t) \neq 0$.

observed that eventually the amplitude of E(t) drops below the modulation threshold of the diode laser and the correlation result, as measured by the linear detector array, goes to zero before the amplitude of E(t) goes to zero.

The software permits the user to pause the minimizing process of the closed loop system and observe the output of the linear detector array. We have often observed a flat response from the correlation result when the oscilloscope plainly indicates that E(t) is still far from its minimum value. This problem might be resolved by replacing the present source with a laser device that has a minimum modulation threshold of 0.5 V peak-to-peak or less. Another alternative is to use a programmable amplifier. The amount of amplification would be a function of E(t) as measured on the oscilloscope. Care would need to be taken to ensure that the amplified signal (specifically the desired signal s(t)) does not overdrive the laser.

7.1.2 Making Use of Spatial Information from Correlation. The spatial characteristics of the time integrating correlation data are essential to the optimal performance of the optical processor. The theory of operation assumed that the location of correlation peaks obtained with the detector array in the time integrating correlator would correspond to specific time delays. Figure 13 shows actual data for correlation peak location as a function of a fixed delay between $n_1(t)$ and $n_2(t)$ during closed loop operation. The data in this figure was collected by reading off the correlation peak location from the detector array for different phase delays, before the system had a chance to adaptively cancel $n_1(t)$. The trend in this data shows that as the delay changes, the correlation peak location also changes linearly in pixel number. The error bars represent the range of pixels over which the correlation peak is likely to occur for a given delay. Multiple sets of data were taken for each delay shown, and the error bars are defined as two standard deviations about the mean of each data set. If the optical processor uses the data from the detector array directly to select time delays for the space integrating correlator, there is a high probability the wrong delay will be selected. For example, a peak at pixel 245 might represent a delay ranging from -90 to +45 degrees. Therefore, in the present configuration the system's computer uses the pixel location information to set a range for possible delay values. This range is based on the possible time delays a pixel location can represent. The data shown in Figure 13 is used to determine this range.

Future efforts should include reducing this range of possible delays. These shifts in peak location may be caused by system noise in the amplifiers and subtraction circuitry. Another possibility is in the AO modulators which may be distorting the signal delay in the transducer circuitry. However, the most likely cause of the wide range of peak locations for a given delay is the subtraction of y(t) from $n_1(t)$. The subtraction of two sinusoids of the same frequency with unique amplitude and phase yields a third sinusoid at the same frequency, but with amplitude and phase information which differs from the initial functions. It can be shown that the phase of the resultant sinusoid is a function of the amplitude and phase of the initial functions. This amplitude dependence of the phase produced in the subtraction circuitry could give rise to the variation of correlation peak locations at a given delay.

To test this theory we removed the signal y(t) from the input to the diode laser. Hence, the laser is now modulated only by $s(t) + n_1(t)$. The AOM is modulated by $n_2(t)$. We record the correlation peak location as a function of delay between $n_1(t)$ and $n_2(t)$, as described in Section 7.1.2. With y(t) removed, we find that the correlation peak moves in a deterministic manner as a function of delay. In fact, for a given delay, the correlation peak will be found at the same exact position to within one pixel. For example, a correlation peak at 275 corresponds to a delay of 90 +/- 6 degrees.

A possible method to eliminate the effects of y(t) on the correlation peak location is to add a routine in the computer program which switches off the input of y(t) when the amplitude of E(t) increases over threshold. A programmable switch would be added at the y(t) input. This would allow the computer to better use of the spatial information of the correlation data at the expense of increased processing time and system complexity.

7.1.3 System Noise. System noise ultimately limits the ability of the system to accurately estimate and cancel a jamming signal. The system continually monitors the linear detector output and initiates the adaptive process when the peak to peak amplitude of the correlation peak changes by more than a user defined threshold or when the location of the correlation peak moves by several pixels. Hence, noise which causes the correlation peak to vary in amplitude or spatial location on the linear detector array is misinterpreted by the system as a change in the multipath environment. Ideally, a change in the correlation result would indicate a change in the delay or amplitude of the received jamming signal. However, we have observed that system noise is often the cause of initiating the adaptive process.

There are several possible sources for noise in the correlation result. One initially suspects the diode laser, AO modulator, or linear detector array as a possible noise sources. However, as explained in Section 7.1.2, y(t) may also be noisy. Therefore, the CW, AOSLM, AO modulator, photodiode and amplifier circuitry may also be sources of system noise. The exact source of this noise will need to be identified, characterized, and addressed in the Phase II development.

7.2 Future Work

7.2.1 Future Measurements with Single Channel Processor. The Phase II development of the optical processor is to design and fabricate a multichannel system using this single channel system as a baseline design. The multichannel adaptive optical processor (MADOP) will be designed to provide the ability to simultaneously cancel up to four distinct multipath sources. However, the single channel processor must be further characterized before the MADOP design is finalized. We plan to perform the following tasks on the single channel system during the initial stages of the MADOP design effort:

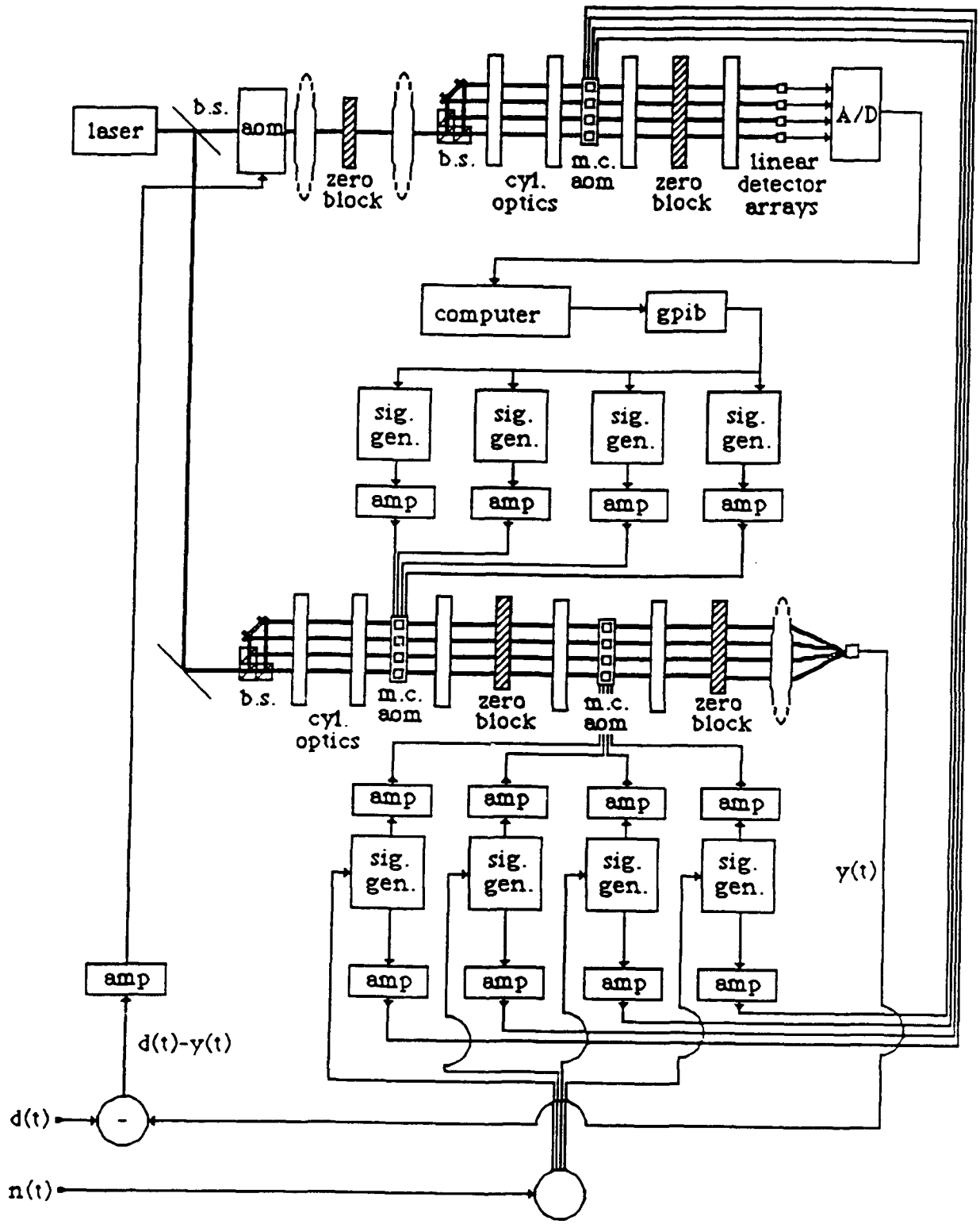

Figure 14: Preliminary architecture for multichannel adaptive optical processor in Phase II effort.

a. Test the ability of the system to adaptively cancel a monotone, two delay test signal.
b. Test the ability of the system to adaptively cancel a wide bandwidth (10 MHz) single delay test signal.
c. Maximize the cancellation ratio of the closed loop system. Identify key components to achieve 30 dB cancellation of the above mentioned signals.
d. Identify and reduce noise sources.

Most of these tasks are somewhat dependent on the signal generation equipment available to the research team at the Photonics Center. The Radar Signal Simulator (RSS) should be capable of generating a two channel output of a wideband RF signal with phase control between the two channels. (The RSS has been developed by General Electric, Syracuse, NY under contract with the Rome Laboratory Command, Control, and Communications Directorate.)

7.2.2 Multichannel Optical Processor (Phase II) As mentioned previously, a follow-on effort to the work described here is the design and fabrication of a multi-channel optical processor which has the capability of simultaneously processing up to four jamming sources, with each jammer possibly generating its own unique set of multipath returns. Initial plans call for the construction of a two channel system that is able to be upgraded to a four channel system. Such a system will rely heavily on the integration of multichannel AO devices into the system architecture that has been presented here. A sample architecture is shown in Figure 14.

The MADOP will require three multichannel AO devices. The first will be used in the time integrating correlator, with each AO channel receiving input from a separate auxiliary antenna. The laser source in this correlator will continue to be driven by input from the main antenna. However, the beam will need to be split several times, once for each system channel. The beamsplitter configuration shown in Figure 14 should provide four equal intensity beams at the proper separation from one another. The second multichannel AO device will be used as the SLM in the optically tapped delay line. Each AO channel will be separately driven by output from the computer. Using an optical system similar to that shown in Appendix B, the spatially modulated light will be incident onto the third multichannel device, whose separate channels are also driven by the auxiliary antennas.

The interface between multiple linear detector arrays, multiple data acquisition boards, and multiple computer controlled signal generators is expected to be one of the most difficult aspects of this project. Perhaps one way of reducing the complexity of the detector/computer interface would be to use a single high resolution (1 x 2048 pixels) array and cause the input beams to strike the array at unique locations. For example, let channel 1 be imaged on pixels 1-256, channel 2 on pixels 257-512, channel 3 on pixels 513-768, ..., and channel 8 on 1792-2048. If this method is

used, then for imaging purposes, it might be more convenient to use multiple single channel AO devices rather than a single multichannel device.

7.3 Conclusions. This report has documented the Phase I in-house effort to develop an optical processor to adaptively cancel sidelobe jamming. The system described in this report has demonstrated the ability to achieve a 15.2 +/- 2.4 dB adaptive cancellation of a monotone, single delay test signal over a range of 1-5 MHz in the presence of a desired monotone signal. The open loop optical system has proven capable of providing a 30.2 +/- 3.9 dB cancellation of the same signal when using operator provided information. To date, key elements of this project have included the characterization and selection of a spatial light modulator system and the development of a software package which assists the minimizing process. This has resulted in the novel use of a two dimensional binary SLM to perform as an enhanced grey scale one dimensional SLM. Additionally, an AO deflector has been demonstrated to provide the grey level dynamic range and spatial resolution required by the system. The results of this single channel testbed will be used in the future development of a multichannel optical processor.

References

1. Welstead, S.T., M.J. Ward, "Hybrid electro-optic processor", RL Final Report, RL-TR-91-164 (1991).

2. Welstead, S.T., "Algorithms for optical processor", RL Final Report, RL-TR-91-34, (1991).

3. Widrow, B., S.D. Stearns, Adaptive Signal Processing, Prentice-Hall, Inc., Englewood Cliffs, N.J., (1985).

4. Brent, R., Algorithms for Minimization without Derivatives, Prentice-Hall, Englewood Cliffs, N.J., (1973).

5. Berg, N.J., J.N. Lee, Acousto Optic Signal Processing, Marcel Dekker, Inc., New York, (1983).

6. Kellman, P., Time Integrating Optical Signal Processing, Stanford University, Ph.D., (1979).

7. Blanchard, D.M., M.J. Ward, "Characterization of liquid crystal displays for optical signal processing applications," RL Technical Report RADC-TR-89-226, (1989).

8. Welstead, S.T., M.J. Ward, D.M. Blanchard, G.A. Brost, S.L Halby, "Adaptive signal processing using a liquid crystal television," SPIE Proc., **1154**, pp 244-252, (1989).

9. Ward, M.J., C.W. Keefer, D.J. Grucza, S.T. Welstead, "Comparison of spatial light modulators for multipath delay estimation", OSA Technical Digest, **14**, pp 149-152, (1990).

10. Welstead, S.T., M.J. Ward, "Extended Dynamic Range One Dimensional Spatial Light Modulator," U.S. Patent Pending, (1989).

APPENDIX A: Detailed listing of equipment used, in reference to Figure A1.

a. GaAlAs diode laser (670 nm), D.O. Industries, 067-02-4.
b. 45 degree line generating lens, Mathews Optical, M45.
c. 150 mm focal length plano-cylindrical lens, 50 mm x 60 mm.
d. 40 MHz acousto-optic deflector, IntraAction Corp., ADM-40.
e. 300 mm focal length biconvex lens, 3" dia.
f. Iris aperture, 2 mm dia. clear aperture.
g. 300 mm focal length plano-cylindrical lens, 50 mm x 60 mm.
h. 300 mm focal length plano-cylindrical lens, 50 mm x 60 mm.
i. 512 element linear detector array, Reticon, RL0512SAQ-011.
j. Zenith 248 PC-compatible computer,
k. Synthesized sweeper, Hewlett-Packard, 83623A.
l. Synthesized RF signal generator, Fluke, 6060.
m. Two channel synthesizer, Hewlett-Packard, 3326A.
n. 3 Watt, 37 dB amplifier, ENI, 403LA.
o. Frequency doubled, diode pumped Nd:YAG laser (531 nm), ADLAS, DPY 215.
p. Spatial filter, Newport Corp., 910.
q. 75.6 mm focal length biconvex lens, 2" dia.
r. 300 mm plano-cylindrical lens, 50 x 60 mm.
s. 40 MHz acousto-optic deflector, IntraAction Corp., ADM-40.
t. 300 mm focal length plano-cylindrical lens, 50 mm x 60 mm.
u. 500mm focal length plano-convex lens, 2" dia.
v. Iris aperture, 6mm dia. clear aperture.
w. 50.2 mm focal length bi-convex lens, 2" dia.
x. 300 mm focal length bi-convex lens, 2" dia.
y. 40 MHz acousto-optic modulator, IntraAction Corp., AOM-40.
z. 150 mm focal length plano-convex lens, 2" dia.
aa. Adjustable slit, 0.4 mm x 10 mm, Oriel Corp., 77263.
bb. 100 mm focal length bi-convex lens, 2" dia.
cc. 100 mm focal length plano-convex lens, 2" dia.
dd. Photodiode, 40 MHz BW.
ee. 40 dB amplifier, TronTech, W40C.
ff. 1 Watt, 34.5 dB amplifier, Amplifier Research, 1W1000.
gg. 3 Watt, 37 dB amplifier, ENI, 403LA.
hh. Spectrum analyzer, Tektronix, 2710.
ii. Digitizing oscilloscope, Tektronix, 11403; two channel amplifier, Tektronix, 11A52.
jj. Signal processor, IntraAction Corp., ME-40G.
kk. Signal processor, Intra-Action Corp., ME-40RG.

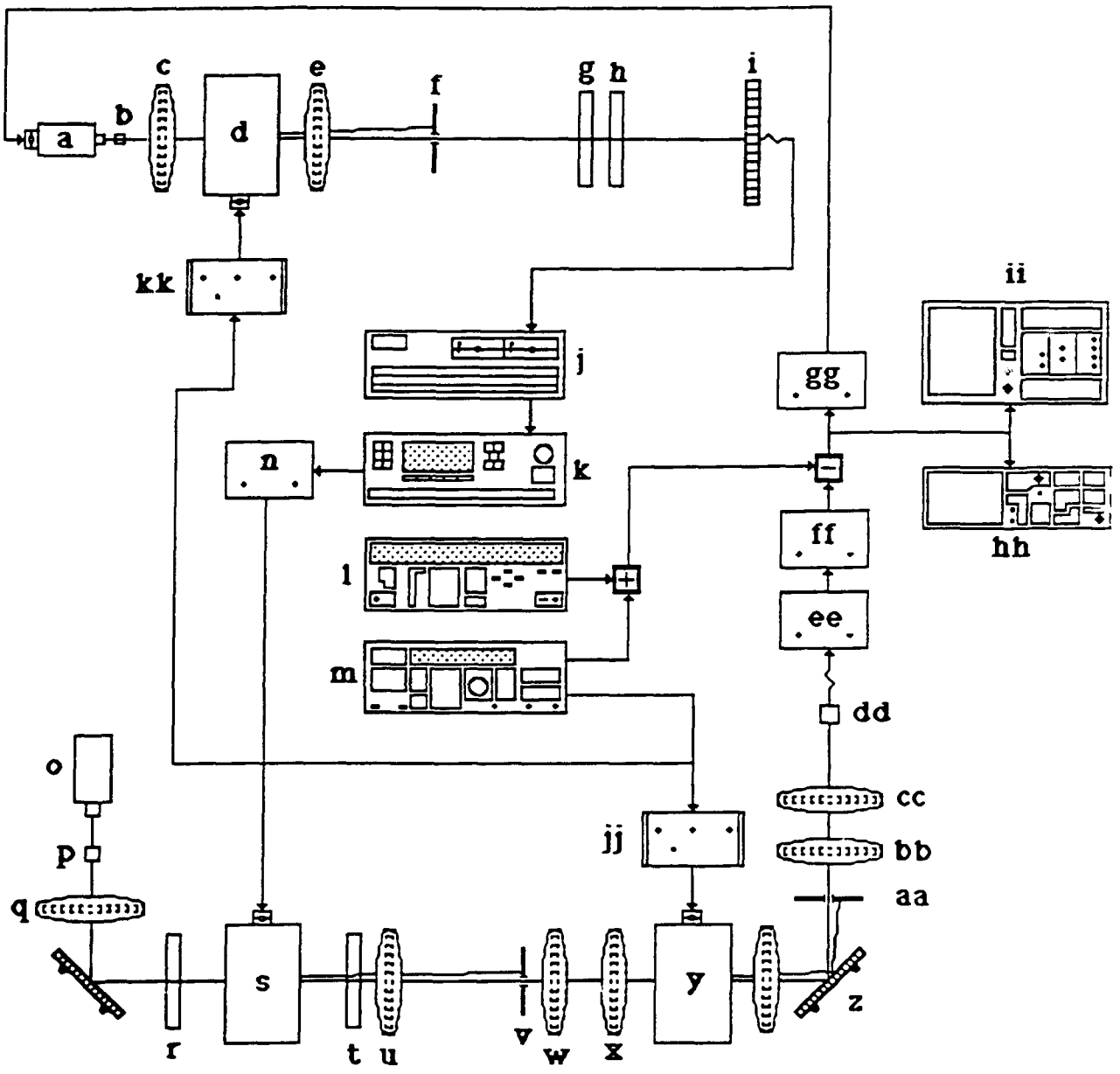

Figure A1: Architecture for single channel adaptive optical processor. Specific equipment specifications are coded to the letters on the figure.

APPENDIX B

Detail of Optical Design

Detailed drawings of the optical architecture for the adaptive optical processor are shown on the next two pages. Note that lateral displacements of optical elements from the optical axis (OA) are not shown in these drawings. The only dimensions shown are the longitudinal (along the OA) dimensions. Lateral displacements arise because the acousto-optic devices redirect the first diffracted order by 6 mrad from the OA. The optical elements in the architecture shown should be moved laterally, so as to ensure that these diffracted beams remain centered. Each optical element is coded to the equipment listing in Appendix A to provide such details as focal lengths, radii, etc.

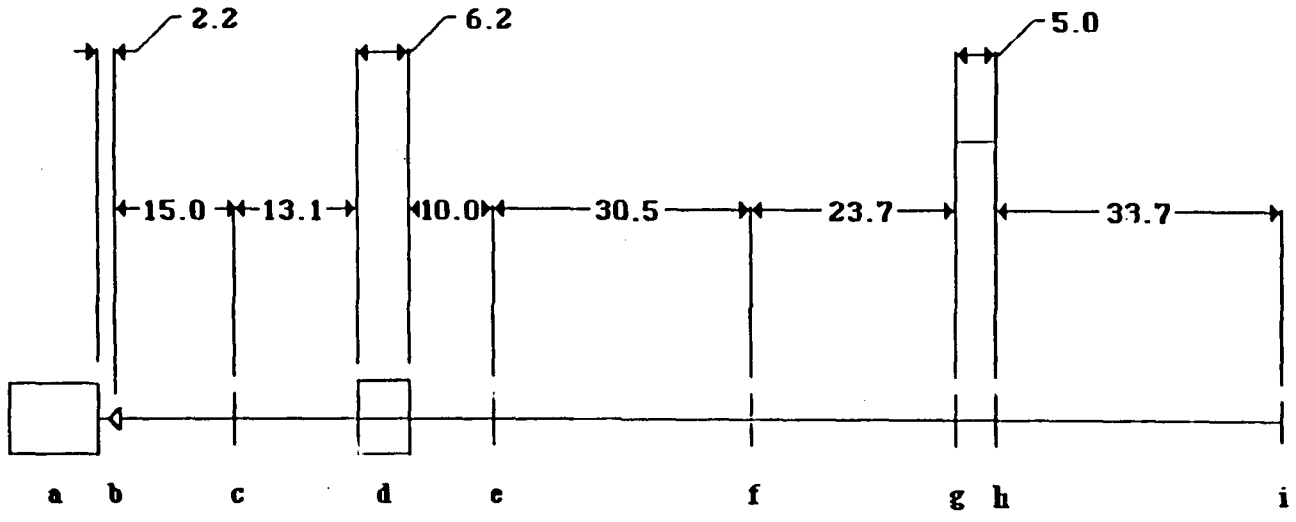

TIME INTEGRATING CORRELATOR	
4 FEB 91-mjw	SCALE: 3/16"=4 cm

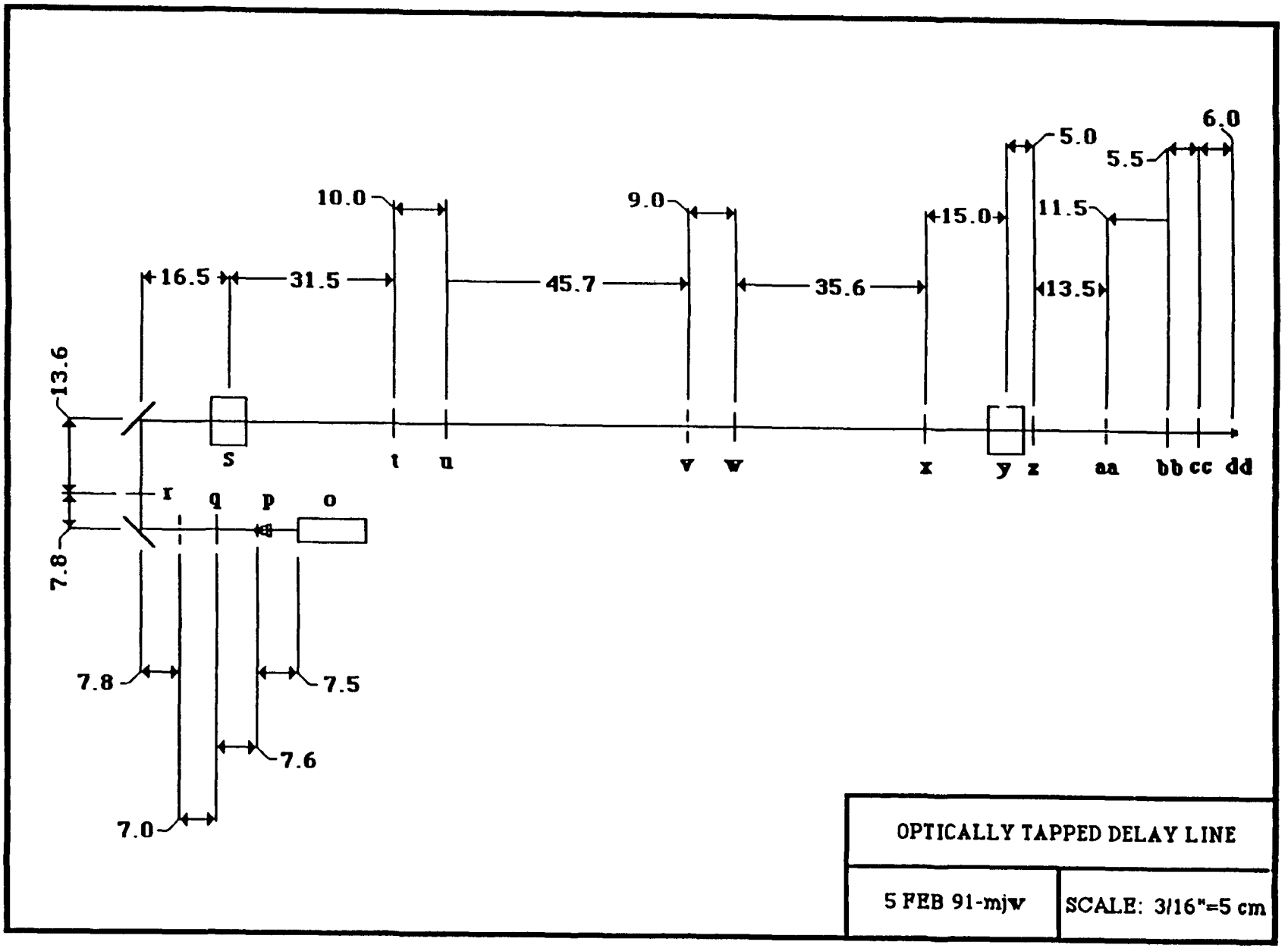
13.6
16.5
31.5
10.0
45.7
9.0
35.6
15.0
5.0
11.5
13.5
5.5
6.0
s
t
u
v
w
x
y
z
aa
bb
cc
dd
r
q
p
o
7.8
7.8
7.5
7.6
7.0
OPTICALLY TAPPED DELAY LINE
5 FEB 91-mjw
SCALE: 3/16"=5 cm

MISSION

OF

ROME LABORATORY

Rome Laboratory plans and executes an interdisciplinary program in research, development, test, and technology transition in support of Air Force Command, Control, Communications and Intelligence (C^3I) activities for all Air Force platforms. It also executes selected acquisition programs in several areas of expertise. Technical and engineering support within areas of competence is provided to ESD Program Offices (POs) and other ESD elements to perform effective acquisition of C^3I systems. In addition, Rome Laboratory's technology supports other AFSC Product Divisions, the Air Force user community, and other DOD and non-DOD agencies. Rome Laboratory maintains technical competence and research programs in areas including, but not limited to, communications, command and control, battle management, intelligence information processing, computational sciences and software producibility, wide area surveillance/sensors, signal processing, solid state sciences, photonics, electromagnetic technology, superconductivity, and electronic reliability/maintainability and testability.